Astron. Astrophys. 278, L19–L22 (1993)

ASTRONOMY AND ASTROPHYSICS

Letter to the Editor

Optical imaging of the gravitational lens system B 1422 + 231

M. Remy[1,3], **J. Surdej**[1,4], **A. Smette**[1,2], **and J.-F. Claeskens**[1]

[1] Institut d'Astrophysique, Avenue de Cointe 5, B-4000 Liège, Belgium
[2] European Southern Observatory (La Silla), Casilla 19001, Santiago, Chile
[3] Also Aspirant (Fonds National de la Recherche Scientifique, Belgium)
[4] Also Maître de Recherche (FNRS, Belgium)

Received July 15, accepted August 3, 1993

Abstract. Direct optical images (Bessel V, R and Gunn i; average seeing of 0.88″) of B1422+231, obtained in March 1993 at ESO (La Silla), have been decomposed by fitting multiple Point Spread Functions. We detect the optical counterparts of the four known radio point-like components. No additional optical image is found, but due to the compactness of the configuration, our detection limit for additional point sources is rather low (19.3 in R). The deduced positions and photometry of the four optical components agree pretty well with the radio and IR observations and this study provides further evidence supporting the gravitational lens origin of B1422+231.

Key words: gravitational lensing – quasar: ind.:B1422+231

1. Introduction

The radio-loud quasar B1422+231 (z = 3.62) has been reported to be a gravitational lens (GL) candidate in the framework of a VLA mapping of flat-spectrum radio sources by Patnaik et al. (1992). It appears on VLA radio maps as a four-components object within a circle of 1.3″ in diameter. Those authors have clearly demonstrated that the point sources have similar spectral index and polarimetry. Its GL nature has then been confirmed by direct imaging in the infrared (Lawrence et al. 1992). These conclusions strongly suggested that the four images consist of a gravitational mirage produced by a yet undetected massive deflector. In this paper, new evidence supporting the GL origin of B1422+231 is presented from direct imaging in the optical.

2. Observations

In the framework of the ESO Key Programme : "Gravitational Lensing" (Surdej et al. 1992), frames have been obtained during a 4 nights run on March 19–23 1993 with the direct camera and CCD#8 (RCAD 5103-2-6) at the Cassegrain focus of the ESO/MPI 2.2m telescope. The pixel size is of 15 μm, which represents 0.1752″on the sky. B1422+231 has been observed under average seeings of 1.08″and 0.68″, respectively on the second and third nights of the run (see Fig. 1 for a finding chart). The frames have been taken through the Bessel V, R and Gunn i filters. All the observations have been obtained under an average airmass of 1.65 ± 0.02. The integration times range from 3 to 10 min. See Table 1 for details of the observational log book. As the conditions were photometric, the Johnson UBVRI standard stars PG1633+099 B & C (Landolt 1992) have been observed at the end of the nights.

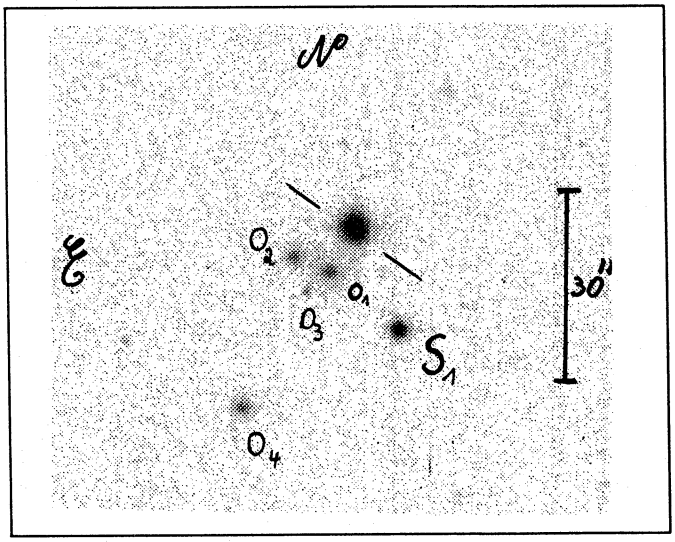

Fig. 1. R image (t_{int} = 10min) of the field around B1422+231. On the sky, the neighbourhood of B1422+231 is crowded with diffuse objects (the only point-like object is S1). Their magnitudes are given in Table 2.

3. Data calibration and analysis

In order to check for the recently reported non-linearity problem of some CCDs at La Silla and in particular CCD#8 (Magain et al. 1992; Remy et al. 1992; Schwarz and Abbott

Send offprint requests to: M. Remy

1993), pairs of equally exposed flat-fields have been obtained for various exposure levels. The variance of the quotient of the two flat-fields of the pair should be a linear function of their common exposure level. This has actually been found to be the case as shown in Fig. 2. The corresponding curve (called variance curve) is indeed well approximated by a straight line: the maximum deviation is less than 2%. This test gives us a good confidence in the linearity of CCD#8. By this method, we also deduced a conversion factor of 4.10 e^-/ADU (Adapter Unit) and a read-out-noise of 26 e^-.

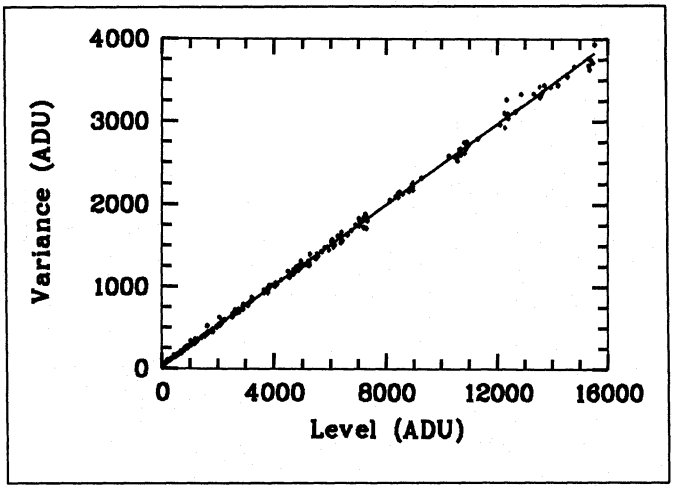

Fig. 2. Variance curve of CCD#8 during our observing run.

The dome flat-fields appear to be stable throughout the complete run and an average of ten of them (with levels ≈ 4000 ADU) has been constructed for each filter. Column offsets of the CCD have been removed using an average template deduced from the flat fields. The subtraction works well within the whole frames if the sky level is above ≈ 300 ADU. Otherwise, this method only removes adequately the offsets in the well exposed parts of the frame. It also creates "anti-offsets" in the sky when its level is very low. The frames have then been bias subtracted and flat-field corrected. This reduction process has also been applied to some sky flat fields (unusable for other purposes) and the flat field correction appears to be as good as 1%, except on the Gunn i frames where some fringes are not so well corrected by the dome flat fields.

The good oversampling of our data allows us to analyse these in the following way. For each frame a numerical model for the point spread function (PSF) has been constructed using well isolated point sources in the field. In order to model the PSF as well as possible we have used numerical profiles rather than approximate analytical Moffat ones. Four such numerical profiles were then fitted to each frame of B1422+231 leading to a minimum χ^2. In the fitting process, the positions and peak intensities were allowed to vary. In all cases but the first R frame (saturated), the differences between the real and model images expressed in terms of noise standard deviation fall within the [-5.,+5.] interval and do not present strongly correlated values. No significant pattern is observed on an average image of the residuals. The resulting values obtained for the fitting parameters allow us to deduce a reliable photometry and a precise relative astrometry.

Table 1. Log book of the observations. The universal date is given in the second column. The universal time corresponds to the *beginning* of the observation. Integration time in seconds, seeing and mean airmass are given in the three next columns.

Filter	Date	UT	t_{int} (s)	FWHM	Airmass
R	03/21/93	$7^h16^m11^s.8$	600	1.01″	1.63
V	03/21/93	$7^h29^m38^s.8$	300	1.09″	1.64
R	03/21/93	$7^h37^m40^s.4$	180	0.96″	1.64
R	03/21/93	$7^h43^m55^s.4$	180	0.94″	1.65
V	03/21/93	$7^h49^m58^s.6$	180	1.30″	1.66
V	03/21/93	$7^h56^m10^s.4$	180	1.23″	1.67
i	03/22/93	$7^h13^m43^s.0$	180	0.65″	1.63
i	03/22/93	$7^h19^m30^s.6$	180	0.65″	1.63
i	03/22/93	$7^h24^m48^s.4$	180	0.67″	1.64
i	03/22/93	$7^h30^m29^s.2$	180	0.67″	1.64
i	03/22/93	$7^h36^m01^s.2$	180	0.71″	1.65
i	03/22/93	$7^h41^m45^s.0$	180	0.73″	1.65

3.1. Positions

As shown in Fig. 3, the V frames seem to indicate somewhat different positions for the D image. Nevertheless, during another fitting iteration, we have fixed the relative position of the D images to the average value deduced from the R and i frames. After visual inspection, we do not detect any significant differences in the residuals. Moreover, we have constructed two artificial frames which mimic actual frames (one in R and one in V) using adapted Moffat profiles for the four components and for the two brightest point sources in the field. We have also added an amount of gaussian noise to each pixel (with the standard deviation corresponding to the observed frames). Furthermore we have assumed (1) that the flat-field correction and (2) the sky subtraction were perfect. The imperfection of the PSF model was then assumed (3) to come only from the noise in the parts of the image used to deduce it. We have then processed these artificial images exactly in the same way as the scientific images. As a result of these fits, the derived position of the D component does also reveal some unexpected scatter. It moves on the line towards the brightest component (B) by 0.05″for the red simulation and by 0.10″for the V simulation. As the PSF has not always been determined using the brightest stars in the field one can expect larger values for the dispersion on the deduced positions. The really observed dispersion in the positions of D seems to be twice these values; this could be explained by a failure in one of our assumptions (1), (2) or (3) (see above).

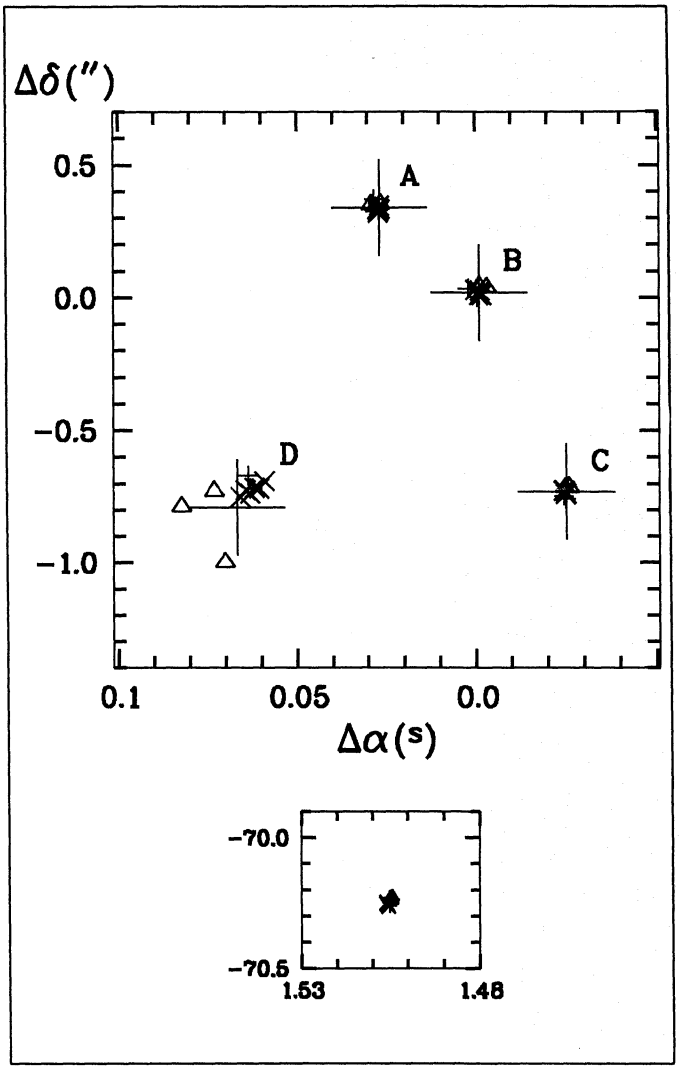

Fig. 3. Upper: relative positions of the four components with respect to bright point sources in the field (a constant offset has been applied in order to get the B component around the origin) (symbols + : R, △ : V and × : i frames). Large crosses represent the radio positions. Lower: we have represented the relative positions of a nearby field star having a brightness similar to that of component B, using the same calibration and scale in (α, δ). The calibration has been obtained by fitting the PSF to individual stars.

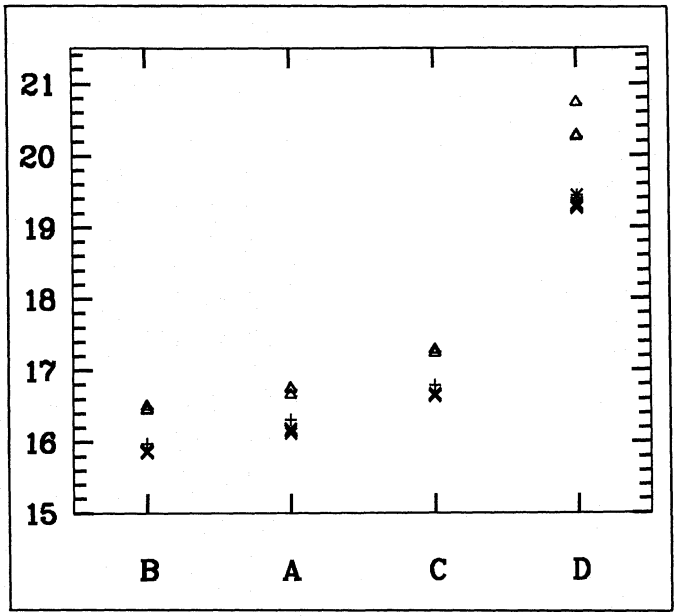

Fig. 4. Photometry of the four components of B1422+231 (+ : R, △ : V and × : i frames).

Table 2. Average magnitudes and relative astrometric positions. The positions and magnitudes of the nearby diffuse objects (O) introduced in Fig. 1 consist of rough estimates: their magnitudes were obtained by integration of the flux inside an aperture of 3″in diameter; they are accurate to 0.2 mag.

	$\Delta\alpha$(s)	$\Delta\delta$(″)	V	R	i
A+B+C+D	–	–	15.54	15.07	14.95
A	+0.028	+0.32	16.71	16.31	16.16
B	+0.000	+0.00	16.46	15.98	15.87
C	−0.024	−0.75	17.26	16.78	16.65
D	+0.067	−0.77	20.42	19.44	19.32
O1	+0.25	−07.1	20.0	19.5	18.8
O2	+0.68	−04.8	20.4	19.9	19.1
O3	+0.54	−10.1	21.6	21.0	20.5
O4	+1.26	−28.3	20.3	20.0	19.4

Nevertheless, these results demonstrate that the observational scatter for the D position is not significant. Regarding the dispersion in the positions of A, B and C, they are comparable with the dispersions in position resulting from a fitting of numerical PSF to isolated point sources having the same brightness. We have superposed in Fig. 3 the radio positions assuming that the centroid of the optical position of the B image exactly coincides with the radio position (as no known absolute astrometric calibration is available for the optical positions). The radio positions of the three other components fall very near the centroids of the optical positions. Thus we can state that all frames are compatible with the presence of four optical point-like images coinciding with the radio ones.

3.2. Photometry

The integrated magnitudes of B1422+231 have been deduced only using first order airmass correction with the La Silla mean absorption coefficients (k_V = 0.11, k_R = 0.03 and k_i = 0.01) and no colour correction. Their average values are given in Table 2.

It is shown in Fig. 4 and Fig. 5 that the dispersion in the magnitudes of the A, B and C components seem to be comparable with the dispersion in the magnitude measurements of point sources having similar brightness. The A, B and C components have clearly the same optical colours. The larger dispersion in the photometry of image D can be attributed to the larger dispersion in its deduced relative astrometry (see above)

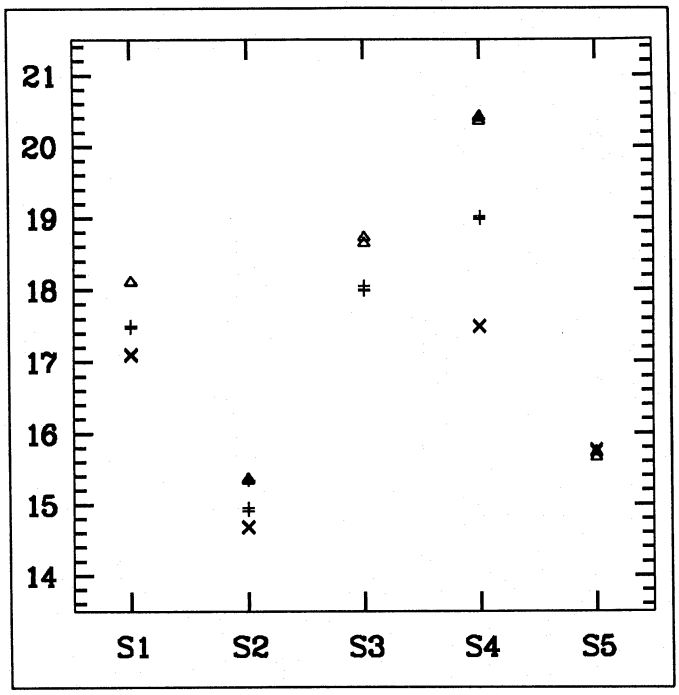

Fig. 5. Photometry of selected point sources in the field of B1422+231 (+ : R, △ : V and × : i frames).

and to the strong correlation existing between its position and peak intensity parameters in the fitting process. Within the error bars, we conclude that the four components have the same brightness ratio in the three used optical filters. The average of the individual values plotted in Fig. 3 and Fig. 4 are listed in Table 2.

3.3. Detectability of a fifth point-like image

In order to check for the presence of a fifth point-like image, we have added a point-like component (deduced from the PSF) to a good R frame around the geometrical centre of the configuration. We have then used our four-components method to fit the resulting image. The observed residuals are definitely significantly worst than the original ones for an added component brighter than R=17.8. For an added component fainter than this value, even if the residuals are not so different, the position and magnitudes are strongly perturbed (for example with a fifth component having R=17.8, D lies 0.39″nearer the B component). Only in the case of an added fifth image fainter than R=19.3 do we obtain displacements that are compatible with the observed dispersion. One can take this value as the detection limit for a point source lying at the centre of the configuration. A fifth point-like object lying elsewhere or an extended object would even be less detectable. Due to the limited resolution in the optical, this detection limit is of course still very low. Nevertheless, we can conclude that our data provide no evidence for the presence of a fifth component brighter than R=19.3 in this configuration.

4. Discussion

The difference between the V integrated magnitude estimated from the POSS survey (V=16.5, Patnaik et al. 1992) and our value (V=15.5) can not be taken as an absolute proof of variability of this bright multiple object: it is saturated on the POSS plates and its estimated magnitude can easily be wrong by 0.5–1.0 magnitude. Futher checks for optical variability of this object should be urgently made since B1422+231 could provide us with an additional GL system to investigate microlensing and/or time delay effects. The evalution of the absolute magnitude from the V magnitude requires an empirical correction (Véron-Cetty and Véron catalogue); more especially as the Lyα+NV emission line is present in the V filter. Without taking into account the correction for the magnification induced by gravitational lensing, we would deduce an absolute magnitude M_V of -30.5 (for V=15.5, H_0 = 50 km s^{-1} Mpc^{-1} and q_0 = 0.5). B1422+231 would therefore appear to be one of the most intrinsically luminous objects in the universe.

In the radio, A and B seem to have very comparable flux (Δm = 0.03) (Patnaik et al. 1992). B appears to be brighter in the IR K band (Δm = 0.19), and this tendency is confirmed in the optical (Δm = 0.31). The discrepancy between the radio, IR and optical differences in magnitude is minimum for B and C (Δm = 0.10), i.e. this is the pair of images for which the colours are the most similar.

Our optical imaging of B1422+231 supports the interpretation that this object is multiply imaged by gravitational lensing. Our data do not indicate any evidence for the presence of a fifth object (R $\leq$ 19.3). It will of course be very important to measure the redshifts of the nearby diffuse objects in the field in order to evaluate their contribution to the GL effect.

Acknowledgements. This research has been supported in part by the contract 90/94-140 "Action de Recherche Concertée de la Communauté Française" (Belgium).

References

Lawrence C.R., Neugebauer G., Weir N., Matthews K. and Patnaik A.R., 1992, *MNRAS* **259**, 5P

Magain P., Surdej J., Vanderriest C., Pirenne B. and Hutsemékers D., 1992, *The Messenger* **67**, 30

Patnaik A.R., Browne I.W.A., Walsh D., Chaffee F.H. and Foltz C.B., 1992, *MNRAS* **259**, 1P

Remy M., Magain P., Smette A. and Surdej J., May 1992, *An updated report on "non linearities" detected with ESO CCDs*, private communication to ESO

Schwarz H.E. and Abbott M.C., 1993, *The Messenger* **71**, 53

Surdej J. et al., 1992, invited paper to the Second D.A.E.C. Meeting on "The Distribution of Matter in the Universe", Eds. G.A. Mamon and D. Gerbal, 97–107

This article was processed by the author using Springer-Verlag TEX A&A macro package 1992.